Malaysian Journal of Chemistry, 2026, Vol. 28(4), 184-203

Esterification of Oleic Acid and Deacidification of *Calophyllum inophyllum* Oil over Lignin-derived Magnetic Carbonaceous Solid Acid

Shamala Gowri Krishnan[1], Zhang Fan[2,3] and Fei-ling Pua[4,5]*

[1]College of Graduate Studies, Universiti Tenaga Nasional, 43000 Kajang, Selangor, Malaysia
[2]Chinese Academy of Sciences, Biomass Group, Key Laboratory of Tropical Plant Resources and Sustainable Use, Xishuangbanna Tropical Botanical Garden, 88 Xuefulu, Kunming, Yunnan Province 650223, China
[3]School of Chemical and Environment, Yunnan Minzu University, Kunming, Yunnan Province 650000, China
[4]Institute of Sustainable Energy (ISE), Universiti Tenaga Nasional, 43000 Kajang, Selangor, Malaysia
[5]Department of Mechanical Engineering, College of Engineering, Universiti Tenaga Nasional, 43000 Kajang, Selangor, Malaysia
*Corresponding author (e-mail: gracepua@uniten.edu.my)

Two magnetic carbonaceous solid acid catalysts, commercial lignin-SO_3H@Fe_3O_4 and EFB lignin-SO_3H@Fe_3O_4, were prepared from commercial lignin and oil palm empty fruit bunch (EFB)-derived lignin, respectively, by simply hydrothermal carbonisation, calcination and sulfuric acid sulfonation steps. The catalysts exhibited high acid density (up to 2.40 mmol/g, including 2.21 mmol -SO_3H/g) and good performance in the esterification of oleic acid with methanol. High esterification rates of 82.6% and 95.6% were achieved at 60 °C within 2 h over EFB lignin-SO_3H@Fe_3O_4 and commercial lignin-SO_3H@Fe_3O_4, respectively, while the catalysts could be reused for at least five times. The catalyst preparation and esterification parameters were optimised by single-factor and Box-Behnken methodologies, respectively. The deacidification of *Calophyllum inophyllum* oil over EFB lignin-SO_3H@Fe_3O_4 was examined. The results of this study demonstrated the feasibility of utilising biomass-derived lignin for the production of magnetic solid acid, which can be used as a green, effective, and practical heterogeneous catalyst in biodiesel production.

Keywords: Lignin, magnetic acid catalysts, hydrothermal, esterification, Box-Behnken

Received: July 2025; Accepted: January 2026

In recent years, global warming has intensified, largely due to the continued consumption of fossil fuels, underscoring the importance of developing potentially alternative and renewable energy resources such as green biodiesel [1]. Biodiesel consists of several medium- or long-chain fatty acid alkyl esters (C12-C18). Its advantages include being non-toxic, having a low sulphur content, high lubricity level, renewable and environmentally benign, and an excellent alternative to liquid fossil fuels [2]. For economics and sustainability, biodiesel is mainly produced from waste or non-edible oils [3, 4] through base-catalysed transesterification. In contrast, non-edible *Calophyllum inophyllum* (CI) is believed to be a potential source for industrial biodiesel production because of its high survival potency in nature (up to 50 years) and high oil yield when compared to the well-known Jatropha. The oil extracted from the seeds of *Calophyllum inophyllum* (CI oil) has the advantages of high heating value and moderately high flash point [5]. However, CI oil contains high free fatty acids (FFAs) with high acid values of 41-60 mg KOH/g, requiring an additional acid-catalysed pre-esterification step before the transesterification reaction [6, 7].

Considering abundant sources and renewable character, lignocellulosic biomass, especially industrial waste lignin, is widely used as one raw material to produce various effective carbonaceous solid acid catalysts [8]. Compared to sugar-based biochar, lignin-based char possibly provided a higher degree of SO_3H functionalisation after sulfonation with H_2SO_4 due to lignin's highly aromatised framework structure [9, 10]. For instance, Pua et al. prepared a novel solid acid catalyst by chemical activation of Kraft lignin with phosphoric acid, pyrolytic carbonisation and sulfonation with sulfuric acid [11]. The prepared catalyst showed an acidity of 1.30 mmol/g (from NaOH titration) and produced a high esterification yield of 96.1% under conditions of 80°C, 5 h and methanol/oleic acid molar ratio of 12. The catalyst was reused for three cycles, with catalyst activity decreased by only 2.6%. Dechakhumwat et al. used corncob-derived lignin residue to produce H_2SO_4 and TsOH sulfonated materials, which also showed considerable activity in the esterification reaction of oleic acid with methanol [12].

Another advantage of using lignin in preparing carbonaceous catalysts is the stable supply of lignin

residue in the paper and pulping industry, which significantly alleviates the problem of waste discharge and thus benefits the economics and sustainability of the industry. In Malaysia's oil palm industry, oil palm empty fruit bunch (EFB) is the second most abundant biomass waste (annual output of about 18 million tonnes in 2007) and contains a substantially higher content of cellulosic portion (~37%) [13–15]. It is more suitable to be used in the paper and pulping industry. However, the rest of the EFB waste pulp, such as black liquor, contains mainly acid-insoluble lignin, which is massively abandoned in the environment or combusted for energy. Only a small portion of the industrial waste lignin is used for commercial applications.

Recently, the intervention of magnetic metal compounds in preparing carbonaceous catalysts has received increasing attention [16, 17]. The iron oxide (Fe-O) presence in the magnetic catalyst serves as Lewis acid and promotes the catalytic activity [18]. The magnetism benefits the recovery and reuse of the solid catalyst and reduces the requirement of centrifugation or filtration, which is time and energy-consuming. The enhanced magnetism of the biomass-derived carbonaceous solid acids may also provide a way to solve the deactivation problem of sulfonated catalyst [19], as possibly formed metal-carbon hybrid linkages may change the surrounding chemical micro-environment of active -SO_3H sites and reduce their leaching in liquid media. For example, the change in the doping ratio of magnetic Zr and Fe complex in sulfonated carbonaceous catalysts ZrFe-SA-SO_3H and ZrFe-CMC-SO_3H significantly altered the activity lost during the reuse of the solid catalysts in oleic acid esterification. As the molar ratio of Fe/Zr in the solid catalysts was 0.5, the esterification activity was decreased by about 32-34% after 5 cycles. In comparison, it dropped to ~9% when the Fe/Zr ratio of 1.0 was executed [20].

In this study, a novel magnetic carbonaceous solid acid was developed using waste lignin as raw material. It exhibited satisfactory activity and improved stability in the esterification reaction of oleic acid and deacidification of CI oil. Some basic physicochemical features of the prepared catalyst were analysed using instrumental characterisation technologies, while the catalyst preparation and esterification parameters were optimised by orthogonal and Box-Behnken methodologies, respectively.

EXPERIMENTAL

Chemicals and Materials

Commercial dealkaline lignin was purchased from Tokyo Chemical Industry, Shanghai, China. Oil palm empty fruit bunch (EFB) fibre was collected from Sztech Engineering Sdn. Bhd. (Shah Alam, Selangor, Malaysia). *Calophyllum inophyllum* (CI) oil was obtained from Indonesia.

Analytical reagents $FeCl_3.6H_2O$ (>99.0%), $FeSO_4.7H_2O$ (>99.0%), ammonium hydroxide (NH_4OH, >99.0%), H_2SO_4 (>98.0%), oleic acid (OA, acid value of 199 mg KOH/g) and methanol (99.9%) were purchased from Xilong Chemical Factory Co., Ltd. (Shantou, Guangdong). Sodium hydroxide (NaOH) and potassium hydroxide (KOH) were purchased from R&M, Malaysia.

Extraction of EFB fibre-derived Soda Lignin

In this work, soda lignin was extracted from the black liquor obtained in the alkaline pulping of EFB fibre. The pulping experiment was conducted in a 2.5 L rotary pulp digester (Institut Perhutanan Tropika Dan Produk Hutan, INTROP, UPM), using 25% (w/v) NaOH aqueous solution and a fibre/liquid ratio of 1:8 was employed. The EFB fibres were cooked at 170ºC for 3 h, and black liquor was recovered after the reaction. The pulp was collected, washed with water and stored at 4ºC.

Lignin was precipitated from the concentrated black liquor by neutralising 200 ml black liquor to pH 6 using 6 M H_2SO_4. 95% ethanol was added to degrade the remaining polysaccharide. The degraded precipitates were filtered and collected in the filtrate to evaporate the ethanol at 80 ºC. The black liquor was re-precipitated by adjusting to pH 2 using 6 M H_2SO_4, filtered and washed thrice with acidified water (pH=2). Lastly, the extracted lignin was oven-dried at 55ºC for 24 h.

The Preparation of Lignin-derived Magnetic Catalysts

Magnetic solid acid catalysts in this work were prepared through three simple steps: (1) hydrothermal carbonisation of lignin with colloidal iron hydroxides, (2) calcination and (3) sulfuric acid sulfonation. The commercial lignin was used as a control raw material to determine the parameters for synthesis preparation, which will be further used to synthesise EFB lignin-derived magnetic acid catalyst.

For a typical procedure, an aqueous solution (50 mL) of $FeCl_3$ (0.02 mol) and $FeSO_4$ (0.01 mol) was loaded in a 3-neck round-bottom flask and pre-heated to 80 ºC using a water bath. Then, 10 ml of 25% ammonia solution was added under vigorous stirring, and after addition, the mixed solution was stirred for another 1 h. The mixture was transferred into an autoclave lined with zirconia oxide (ZrO_2) equipped with a mechanical stirrer (500 mL; FCFD05-30, Jianbang Chemical Mechanical Co., Ltd., Yantai, Shandong Province, China), and 5 g of commercial lignin was loaded into the autoclave. The autoclave was sealed and heated at 180 ºC for 16 h with a stirring speed of 500 rpm. After the reaction, the solid product was recovered and washed thoroughly with deionised water and ethanol several times until the liquid reached a neutral pH. The obtained solid was dried

in an oven at 60 °C overnight and calcined in a tubular furnace of 600 °C for 2 h under flushing nitrogen (200 mL/min) to form magnetic carbonaceous particles. After the hydrothermal carbonisation and calcination reactions ($FeCl_3.6H_2O + FeSO_4.7H_2O + NH_3 \rightarrow Fe_3O_4 + NH_4Cl + (NH_4)_2SO_4 + H_2O$), the carbonised magnetic particles were functionalised using concentrated H_2SO_4 (98%, 50 mL). The magnetic carbonaceous particles and concentrated H_2SO_4 with a 1:10 ratio were added to a sealed glass bottle and heated using a water bath of 80 °C for 6 h. The sulfonated samples were washed repeatedly with hot distilled water (80 °C) until the pH value of the liquid reached neutral, dried in an oven at 60 °C overnight and then ground before use.

The prepared catalysts were used in the esterification process as a response (output) to evaluate reaction efficiency based on the chosen parameters.

Instrumental Characterisation of Solid Lignin and Catalysts

The morphology and elemental compositions of lignin samples and magnetic solid catalysts were examined by scanning electron microscopy (SEM) equipped with electron dispersive X-ray spectroscopy (EDX) (JSM-6010PLUS/LV, JEOL, Japan) in Universiti Tenaga Nasional. X-ray diffraction (XRD) investigation was carried out using X'Pert Pro (PANalytical, Eindhoven, Netherlands) with Cu Kα radiation (λ = 0.154 nm) in the scanning range (2θ) of 10-90°. The average crystallite size (D) of crystalline Fe_3O_4 was calculated from the Debye Scherrer formula:

$$D = 0.89\lambda/\beta\cos\theta \quad \text{(Eq. 1)}$$

where a characteristic diffraction angle of 2θ = 10-90° was used for calculation, and β was the line broadening at the half height of the maximum intensity (FWHM). A physical adsorption analyser (ASAP2020, Micromeritics, USA), using the N_2 adsorption-desorption method, determined the physical porosity of sulfonated catalysts. The specific surface area of the catalyst was calculated at the adsorption branch using the Brunauer-Emmett-Teller (BET) method. The functional groups of the catalysts were detected by Fourier transform-infrared spectroscopy (FT-IR; Nicolet iS10, ThermoFisher Scientific Co., Ltd., Waltham, USA) over the range of 4000 to 400 cm^{-1} with a resolution of 4 cm-1, using the standard KBr disk method to prepare the analysis sample. The magnetisation of the catalyst was measured using a vibrating sample magnetometer (VSM, 7400 Series, Lake Shore Cryotronics, Inc., Westerville, USA) at the Nanocat Lab, Universiti Malaya. The acid density of the catalyst was measured by acid-base titration with 0.1 M NaOH as the titrant.

Catalytic Esterification of Oleic Acid

The performance of the sulfonated catalyst was evaluated by esterifying oleic acid in a sealed glass bottle. The conditions of a typical esterification experiment were 10 g of oleic acid, a methanol/ oleic acid molar ratio of 10, a catalyst loading of 7%, a temperature of 60 oC and a reaction time of 2 h via magnetic stirring at 250 rpm. After the reaction, the solid catalyst was separated by an external magnet (neodymium–iron–boron (NdFeB)), while the collected liquid sample was heated at 70 °C to remove unreacted methanol. Finally, the used catalyst was washed with ethanol and oven-dried at 80 °C for a recyclability study. The acid values (AV) of liquid samples were determined by acid-base titration with 0.1 M KOH, following ASTM D664. Then, the conversion rate in esterification reactions was calculated as the difference between the AV of the esterified samples (AV_{EP}) and that of oleic acid (AV_{OA}).

$$Esterification\ rate\ (\%) = (AV_{OA} - AV_{EP}/AV_{OA}) \times 100 \quad \text{(Eq. 2)}$$

Table 1. The factors and levels for optimisation of catalyst preparation.

Factors	Unit	Level		
		1	2	3
Lignin loading	g	2.5	5	7.5
Hydrothermal carbonisation duration	h	8	16	24
Calcination temperature	°C	400	600	800
Calcination time	h	1	2	3

Table 2. Factors and ranges for the esterification process in the Box-Behnken optimisation study.

Factors	Symbol	Level		
		-1	0	1
Catalyst loading, wt%	A	5	7	9
Methanol to OA, molar ratio	B	8:1	10:1	12:1
Reaction time, min	C	90	120	150

The esterification conditions of oleic acid over EFB lignin-derived solid acid catalyst were optimised using Design Expert Software (version 10.0.3). A Box Behnken methodology was introduced with 3 factors (catalyst loading, methanol to oil molar ratio and duration) and 3 levels for each factor (listed in Table 2), which gave a total of 17 factorial points, with the esterification rate set as the response. The correlation of the response (Y) from randomised experimental runs with varied independent factors (X_i and X_j) was fitted using a full quadratic model:

$$Y = \beta_0 + \sum_{i=1}^{3} \beta_i x_i + \sum_{i=1}^{3} \beta_i x_i + \sum_{i=1}^{3} \beta_{ii} x_i^2 + \sum_{i=1}^{2} \sum_{j=i+1}^{3} \beta_{ij} x_{ij} + \varepsilon \quad \text{(Eq. 3)}$$

where, β_i, β_{ii} and β_{ij} were the regression coefficients for the linear, quadratic, and interactive terms, respectively. β_0 and were the intercept and error, respectively.

Deacidification of *Calophyllum inophyllum* Oil via Catalytic Esterification

Catalytic esterification of degummed CI oil with methanol over EFB lignin-derived catalyst was conducted in a three-neck flask equipped with a reflux condenser, using the following conditions: 60 °C, 120 min, catalyst loading of 9% and different methanol/oil molar ratios. After the reaction, the catalyst was removed using an external magnet. The liquid sample was collected and evaporated at 70 °C to remove excess methanol before product analysis. The KOH titration method determined the AV of as-received and esterified CI oil. The chromatography analysis (GC) of the esterified sample was also performed to examine the formation of methyl esters after catalytic esterification, using 7890A (Agilent Technology, USA) equipped with a capillary column DB-WAX (30 m × 0.32 mm × 0.25 μm) and a flame ionisation detector (FID). The injector, column and detector temperatures were 250, 220 and 280 °C, respectively. The peaks of different methyl esters were identified using GC standards.

RESULTS AND DISCUSSION

The Optimisation of Commercial Lignin-SO_3H@ Fe_3O_4 Catalyst

The influence of four parameters (including lignin loading amount, hydrothermal carbonisation time, and calcination temperature and time) on catalyst preparation was investigated via a single-factor optimisation test to achieve higher esterification rates and greater surface acidity over commercial lignin-SO_3H@Fe_3O_4. The results of single-factor tests were plotted in Fig. 1, while the esterification verification was conducted under the conditions listed in Table 1. Lignin loading of 5 g, hydrothermal carbonisation duration of 16 h, calcination temperature of 600 °C and calcination time of 120 min were used as the parameters of catalyst preparation.

From Figure 1a, it could be seen that the surface acidity was decreased from 2.20 to 1.60 mmol/g with the increase of lignin loading from 2.50 to 7.50 g, while the highest esterification rate of 94.9% was achieved at lignin loading of 5.0 g. Further increasing lignin loading to 7.5 g did not significantly increase conversion; instead, it decreased to 80.2% at an acid density of 1.6 mmol/g. It may be due to the limited active sites on the catalyst, leading to a decrease in the conversion rate [21]. At a lignin loading of 2.5 g, the conversion rate was low due to particle agglomeration and a limited number of active sites exposed to the reactants. A longer hydrothermal carbonisation duration from 8 to 24 h significantly increased the surface acidity of solid acids from 1.80 to 2.60 mmol/g, as shown in Figure 1b. However, higher surface acidity did not certainly result in better esterification performance. At shorter hydrothermal durations, the formation of polycyclic aromatic carbon on the catalyst was limited, thereby limiting the loading of the sulfonic group during the sulfonation process. An esterification rate of >93% was achieved with a hydrothermal duration of ≥ 16 h, and it decreased slightly with further prolonged time. Based on Figure 1c, the elevation of calcination temperature from 400 to 600 °C yielded a drastic increase in both esterification rate (from 74.2% to 95.6%) and

catalyst acidity (from 1.0 to 2.2 mmol/g). This is attributed to the formation of porous structures that allow the loading of sulfonic groups on the catalyst surface, enhancing the catalytic activity [22]. However, a further increase in the calcination temperature does not affect the esterification rate, resulting from the dissolution of Fe_3O_4 and Fe_3C particles during the sulfonation process [23]. Moreover, the catalyst calcined at 800 ºC had lost all acidity and activity. From Figure 1d, the 60-180 min calcination time exerted less influence on surface acidity and the esterification performance of the catalyst. In contrast, a slight reduction in the esterification rate was observed after 120 min of calcination. In summary, the preparation of commercial lignin-SO_3H@Fe_3O_4 was suggested to be conducted under the following conditions: lignin loading of 5.0 g, hydrothermal carbonisation duration of 16 h, calcination temperature of 600 ºC and calcination time of 120 min.

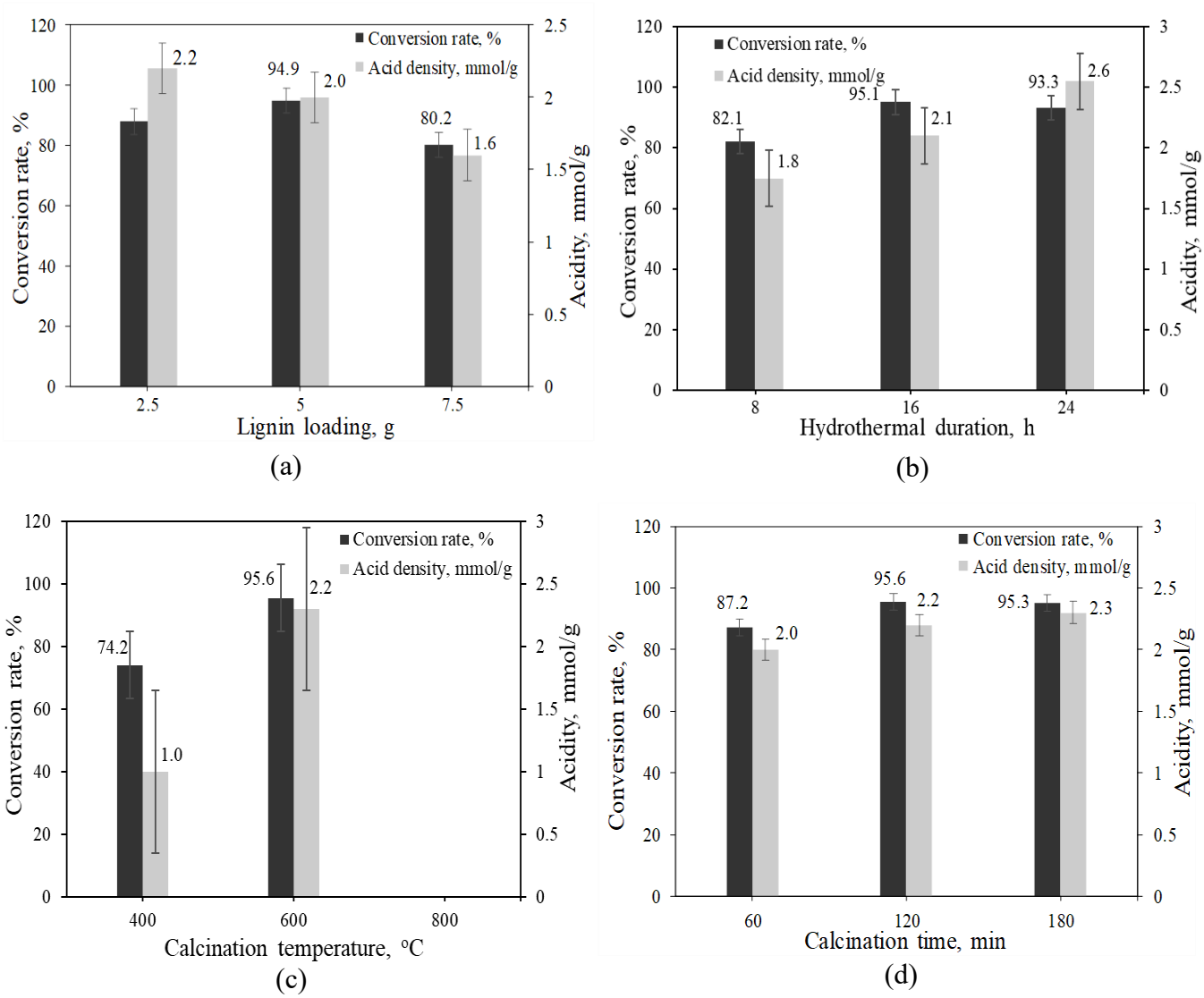

Figure 1. Single-factor investigation of the preparation conditions (a, lignin loading; b, hydrothermal carbonisation duration; c, calcination temperature; d, calcination time) for commercial lignin-SO_3H@Fe_3O_4.

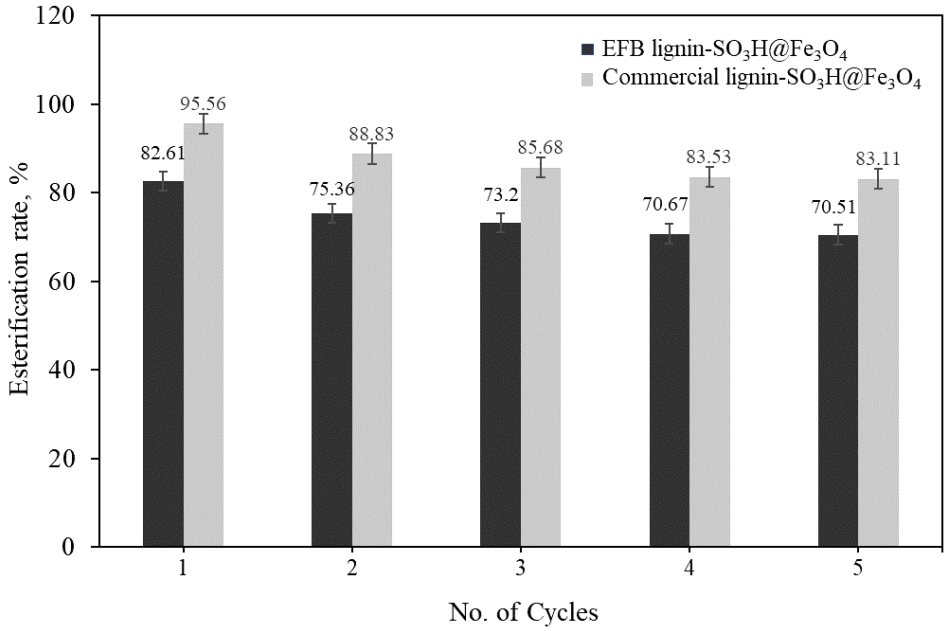

Figure 2. The esterification and recycling performance of EFB lignin-$SO_3H@Fe_3O_4$ and commercial lignin-$SO_3H@Fe_3O_4$ catalysts (Esterification conditions: 60 °C, 2 h, oleic acid of 10 g, methanol/oleic acid molar ratio of 10 and catalyst loading of 7 wt%).

Esterification Performance of Oleic Acid Catalysed by Lignin-derived Magnetic Solid Acids

The performance of both EFB lignin-$SO_3H@Fe_3O_4$ and commercial lignin-$SO_3H@Fe_3O_4$ catalysts was tested using the esterification reaction of oleic acid at 60 °C for 2 h (Figure 2), which received esterification rates of 82.6% and 95.6%, respectively. After the 1st reaction cycle, the used catalysts were recovered with an external magnet, carefully cleaned, dried, and then reused in the esterification reaction. Possibly because of the leaching of acidic active sites from solid catalysts during the esterification reactions, the esterification rates of both catalysts in the 2nd cycle were decreased to 75.4% and 88.8%, respectively. However, from the 3rd cycle onward, the esterification rate was slightly reduced, and the activity of the magnetic acid catalysts remained 93.3-93.7% after 4 cycles (2nd to 5th) compared to the 2nd cycle. The undifferentiated rate of activity reduction for EFB lignin-$SO_3H@Fe_3O_4$ and commercial lignin-$SO_3H@Fe_3O_4$ possibly implied that the two solid acids possessed active sites with the same acidic properties, even though they originated from different lignin materials, and had entirely different porosity. The superiority of the esterification rate over commercial lignin-$SO_3H@Fe_3O_4$ than that of EFB lignin-derived catalyst could be attributed to the higher acidic density of the former catalyst (acidity by titration, 2.40 *vs*. 2.10 mmol/g; -SO_3H content, 2.21 *vs*. 1.49 mmol/g, in Table 3). A lower degree of leaching was observed during the active-site leaching test using EFB lignin-$SO_3H@Fe_3O_4$, with an esterification rate of 48%. The leaching phase of this catalyst was considered low, and this correlated with a reduction in catalyst acidity after 4 reaction cycles. This confirmed that the catalyst has minimal leaching, as the catalyst exhibited a 14.4% reduction in esterification rate after the 4th cycle.

The physicochemical properties and esterification performance of the carbonaceous magnetic solid acids prepared in this work are compared with those in the literature in Table 3. It can be seen that for EFB lignin-$SO_3H@Fe_3O_4$ and commercial lignin-$SO_3H@Fe_3O_4$ catalysts, comparable or even higher oleic acid esterification yields with methanol can be expected at lower reaction temperatures or shorter reaction times. This could be attributed to the higher density of the -SO_3H group and acidic sites over the catalyst surface, especially for commercial lignin-$SO_3H@Fe_3O_4$. More importantly, the solid acids prepared in this work exhibited remarkably improved stability compared to previous literature results, demonstrating the superiority of lignin-derived magnetic acid catalysts as practical solid acid catalysts for biodiesel production and other acid-catalysed synthesis reactions. The magnetic Fe_3O_4 intervention may significantly improve catalyst stability by reducing –SO_3H leaching, and the Fe_3O_4 magnetic core enhances esterification performance. Meanwhile, interactions between Fe_3O_4 and sulfonated lignin can increase the effective acidity of –SO_3H groups and stabilise protonated intermediates formed during esterification.

Table 3. Comparison of the physicochemical properties and esterification performance (oleic acid + methanol) of carbonaceous solid acids prepared in this work with some recently published results.

Catalysts	Surface acidity		Porosity		Magnetic strength (emu/g)	Esterification performance			Refs.
	By S content (mmol SO_3H/g)[a]	By base titration (mmol/g)	Surface area (m^2/g)	Average pore diameter (nm)		Conditions	Yields (%)	Recyclability	
Corncob residue-derived catalyst C-TsOH-10	1.86	0.58	241	3.5	No magnetism	Catalyst loading of 5 wt%, MeOH/OA ratio of 15, 60 °C	80.4	28.8% after 3 cycles	[12]
Microwave-synthesized coal-derived catalyst C250(30)-S75(5)	1.67	1.73	Negligible	-	No magnetism	Catalyst loading of 10 wt%, MeOH/OA ratio of 12, 65 °C, 3 h	98.1	77.2% after 3 cycles	[24]
Bamboo AC-derived catalyst	1.17	1.70	225.71	<10	No magnetism	Catalyst loading of 12 wt%, MeOH/OA ratio of 7, 65 °C, 3 h	91	Activity decreased by ~47% after 3 cycles	[25]
EFB pyrolytic biochar-derived magnetic catalyst MBC02-SO_3H	-	-	38.51	3.17	6.6	Catalyst loading of 5 wt%, MeOH/OA ratio of 8, 150 °C, 2 h	97.6	Not reported	[26]
Alkali lignin alcohothermal carbon-derived catalyst C(HY,E)-S	1.21	8.3	0.03	-	No magnetism	Catalyst loading of 5 wt%, MeOH/OA ratio of 12, 80 °C, 7 h	92.4	84.1% after 4 cycles	[27]
Glucose hydrothermal carbon-derived catalyst C(Glu,W)-S	0.83	4.0	1.8	-			93.3	84.4% after 4 cycles	
EFB lignin-SO_3H@Fe_3O_4	1.49	2.1	56.88	4.55	21.8	Catalyst loading of 7 wt%, MeOH/OA ratio of 10, 60 °C, 2 h	82.6	70.3% after 5 cycles	This work
Commercial lignin-SO_3H@Fe_3O_4	2.21	2.4	0.16	49.7	9.1		97.0	83.3% after 5 cycles	

[a] Surface acidity by S content (mmol SO_3H/g) was calculated using the following formula: Surface acidity (mmol SO_3H/g) = S content in catalyst (wt%) ×1000 / 32.0655

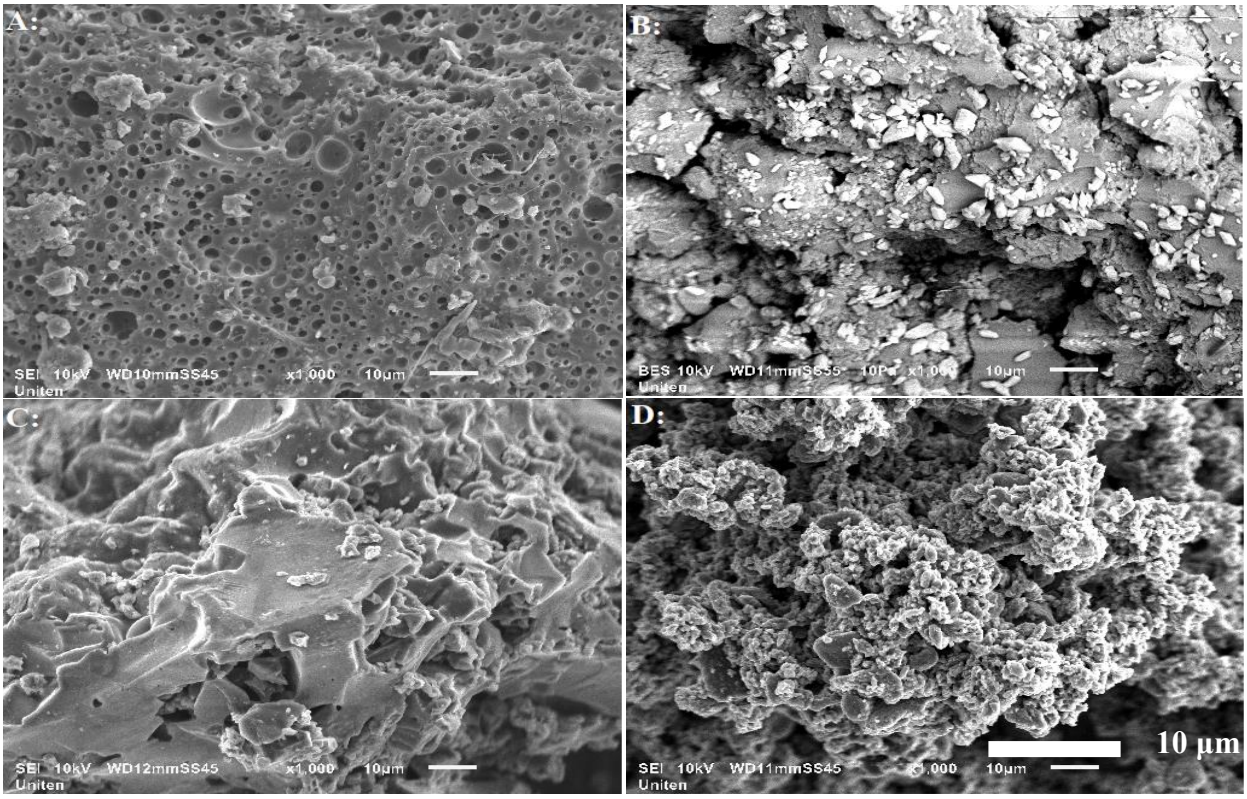

Figure 3. SEM images of (A) EFB lignin, (B) EFB lignin-$SO_3H@Fe_3O_4$, (C) commercial lignin and (D) commercial lignin-$SO_3H@Fe_3O_4$.

Instrumental Characterisation of Lignin-derived Magnetic Solid Acids

The morphology of EFB lignin, commercial lignin, EFB lignin-$SO_3H@Fe_3O_4$ and commercial lignin-$SO_3H@Fe_3O_4$ was identified by SEM analysis (Figure 3). EFB lignin and commercial lignin exhibited both anomalous but different surface morphology. Circular holes with irregular micrometre scales interspersed over the surface of EFB lignin (Figure 3A), while commercial lignin showed a rough surface (Figure 3C). After hydrothermally carbonised and sulfonated with H_2SO_4, the morphology of solid surface was completely fractured. The corrosive effect of strong acid during sulfonation might increase the porosity of the EFB lignin-$SO_3H@Fe_3O_4$ catalyst (Figure 3B) [11]. At the same time, agglomerated particles with spherical shapes were observed on the surface of commercial lignin-$SO_3H@Fe_3O_4$ (Figure 3D). The small irregular particles with a rough surface, indicating iron oxide and the sulfonic group, were successfully formed on the surface of commercial lignin [28]. Meanwhile, the pores on EFB lignin (Figure 3B) were not visible after hydrothermal carbonisation and sulfonation, mainly due to the particles loaded on the EFB lignin surface.

The elemental compositions of EFB lignin, commercial lignin and two lignin-derived catalysts were analysed by EDX in Table 4. EFB lignin consisted of 80.66 wt% carbon (C),17.98 wt% oxygen (O), 1.09 wt% sulphur (S) and 0.27 wt% sodium (Na), while commercial lignin contained 49.04 wt% C, 35.96 wt%, 9.17 wt% S and 5.83 wt% Na. The carbon content was increased to about 52% for the two lignin-derived catalysts, while the presence of iron (Fe) and sulphur (S) contents in EFB lignin-$SO_3H@Fe_3O_4$ (Fe, 17.48 wt%; S, 4.79 wt%) and commercial lignin-$SO_3H@Fe_3O_4$ (Fe, 15.03 wt%; S, 7.10 wt%) might imply the efficient loading of magnetic metal oxide and -SO_3H on the solid catalysts. These results demonstrated that the existence of S in the commercial lignin decreased after the agglomeration of iron particles on its surface. However, the elemental composition of both lignin-derived magnetic catalysts indicates the presence of the SO_3H group after sulfonation [29].

Table 4. Elemental compositions of lignin and the derived solid acids.

Sample	Element Composition (%)				
	Carbon (C)	Oxygen (O)	Sulphur (S)	Sodium (Na)	Iron (Fe)
EFB Lignin	80.66	17.98	1.09	0.27	n.d
Commercial lignin	49.04	35.96	9.17	5.83	n.d
EFB lignin-$SO_3H@Fe_3O_4$	52.71	25.03	4.79	n.d	17.48
Commercial lignin-$SO_3H@Fe_3O_4$	51.49	26.39	7.1	n.d	15.03

n.d = not detected

The magnetism curves of EFB lignin-$SO_3H@Fe_3O_4$ and commercial lignin-$SO_3H@Fe_3O_4$ were determined using VSM, as shown in Figure 4. The curves in the form of a sigmoidal shape confirmed the superparamagnetic properties of the catalysts [20]. The saturation magnetisation values of EFB lignin-$SO_3H@Fe_3O_4$ (Figure 4a) and commercial lignin-$SO_3H@Fe_3O_4$ (Figure 4b) were 21.79 and 9.14 emu/g, respectively, although the Fe content was slightly higher in EFB lignin-derived catalyst (Table 4). The magnetism of the catalysts prepared in this work was comparable to previous literature, like 14.4 emu/g for magnetic carbonaceous acid catalyst derived from glucose [30] and 8.9 emu/g for biomass-based FCHC-SO_3H catalyst [31]. It demonstrated that an external magnetic force could easily separate both EFB lignin-$SO_3H@Fe_3O_4$ and commercial lignin-$SO_3H@Fe_3O_4$ could be easily separated from the reaction mixture.

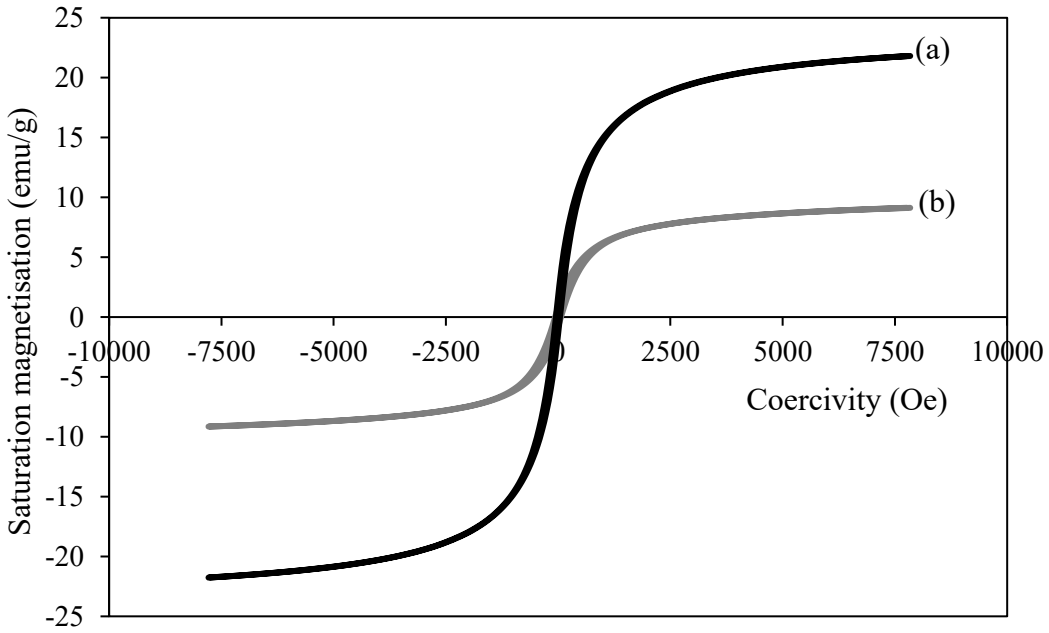

Figure 4. The magnetisation curve of (a) EFB lignin-$SO_3H@Fe_3O_4$ and (b) commercial lignin-$SO_3H@Fe_3O_4$.

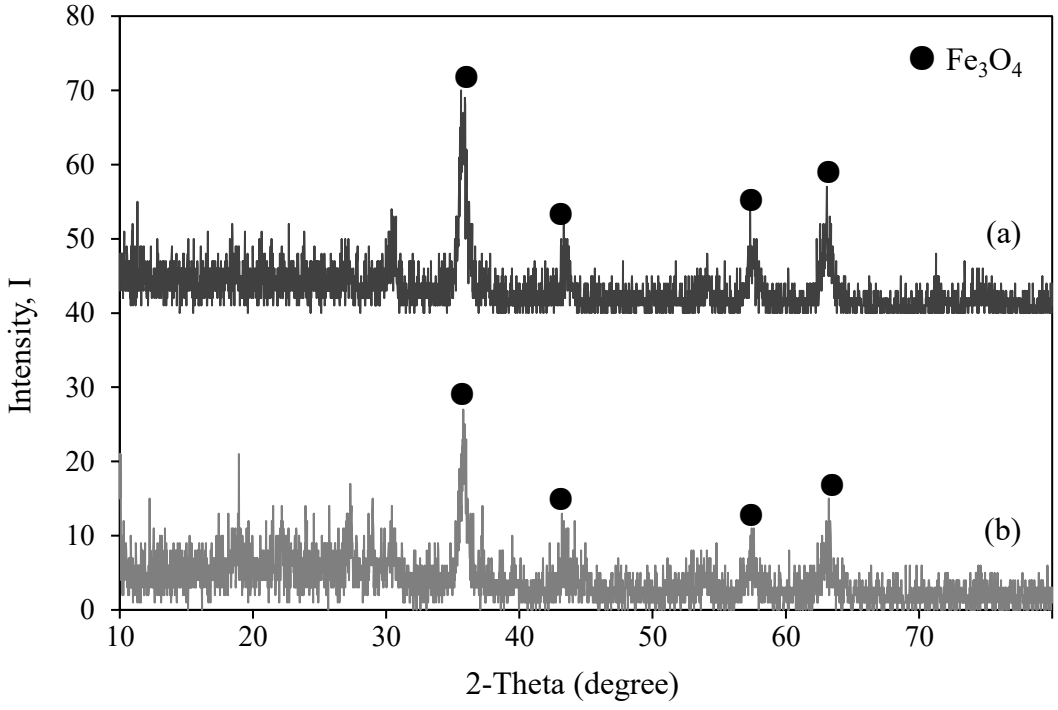

Figure 5. XRD patterns of (a) EFB lignin-SO_3H@Fe_3O_4 and (b) commercial lignin-SO_3H@Fe_3O_4.

XRD characterised the crystalline structures of lignin and two lignin-derived catalysts in Figure 5. The XRD patterns of both raw EFB lignin and commercial lignin presented in Figure S1 with broad diffraction peaks between 2θ 20° to 45°, which are assigned to the 002 planes indicated the existence of carbon in both lignin [32]. XRD patterns of both EFB lignin-SO_3H@Fe_3O_4 (Figure 5a) and commercial lignin-SO_3H@Fe_3O_4 (Figure 5b) exhibited characteristic signals of Fe_3O_4 (ICSD: 98-011-1285) at 2θ = 35.8°, 43.5°, 57.3° and 63.1°, and could be attributed to the formation of Fe_3O_4 cubic spinel structure. Similar peaks were identified in the magnetic lignin-based carbon nanoparticle (MLBCN) reported by Ma et al. [33], which suggests Fe_3O_4 cubic spinel structure in the catalyst. The crystalline sizes of Fe_3O_4 were 13.25 and 15.15 nm, respectively, for EFB lignin-SO_3H@Fe_3O_4 and commercial lignin-SO_3H@Fe_3O_4.

Nitrogen adsorption-desorption isotherms of the two lignin-derived catalysts are shown in Figure 6. The specific surface area and pore volume were determined as 0.384 m^2/g and 0.001 cm^3/g, respectively, for EFB lignin, and 0.112 m^2/g and 0.038 cm^3/g for commercial lignin (Figure S2). However, after hydrothermal carbonisation and sulfonation, EFB lignin-SO_3H@Fe_3O_4 catalyst (Figure 6a) exhibited significantly increased specific surface area of 56.88 m^2/g and larger pore volume of 0.06 cm^3/g, while the porosity of commercial lignin-SO_3H@Fe_3O_4 (Figure 6b) remained negligible (BET surface area of 0.16 m^2/g). The average pore diameter was sharply reduced from 202 nm of EFB lignin to 4.55 nm of EFB lignin-SO_3H@Fe_3O_4, while it was remarkably enlarged (49.7 *vs*. 5.37 nm) after the carbonisation, calcination and sulfonation of commercial lignin. It demonstrated that the porosity of commercial lignin-SO_3H@Fe_3O_4 was mainly composed of a mesoporous structure, while more micropores were formed during the preparation of EFB lignin-SO_3H@Fe_3O_4. The formation of micropores was possibly contributed by the release of volatile gas during calcination [29] or the sulfonation process, while similar results were reported previously by Yang *et al.* [27]. In that work, the sulfonation of alcohothermal biochar derived from TCI dealkaline lignin and cellulose dramatically increased the BET surface area from 0.3 and 10.3 to 221.9 and 89.2, respectively, while the sulfonation of alcohothermal biochar derived from HY alkali lignin and glucose, as well as the sulfonation of hydrothermal biochar derived from TCI lignin, provided less or slightly adverse influence on the porosity of the obtained carbonaceous solid acids

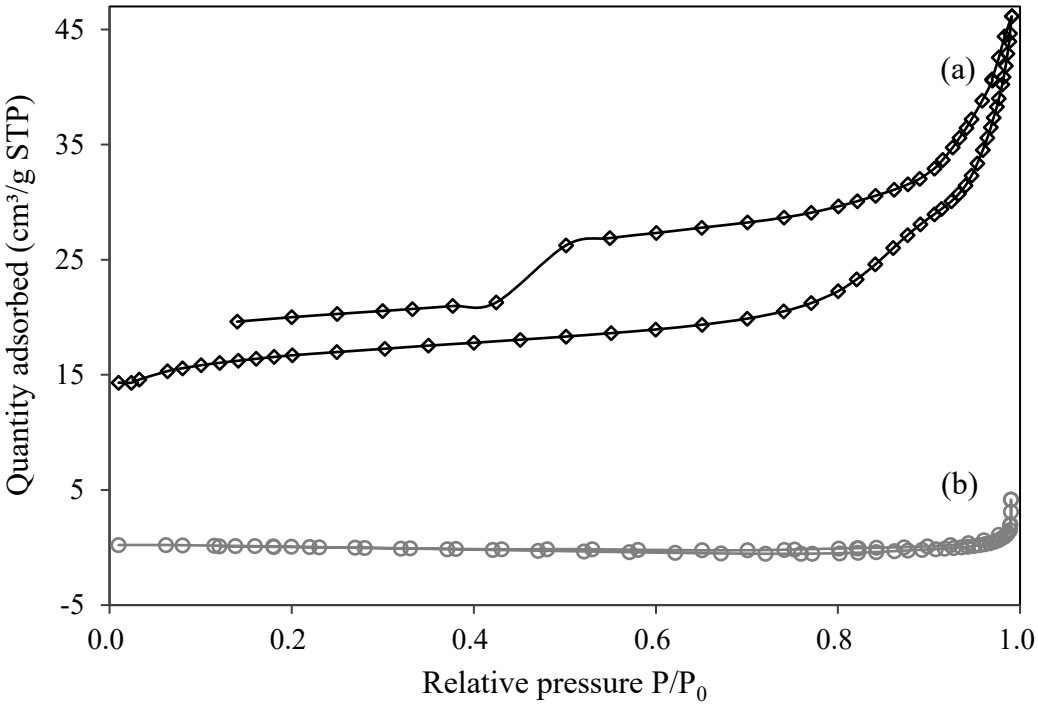

Figure 6. Nitrogen adsorption/desorption isotherms of (a) EFB lignin-SO_3H@Fe_3O_4 and (b) commercial lignin-SO_3H@Fe_3O_4.

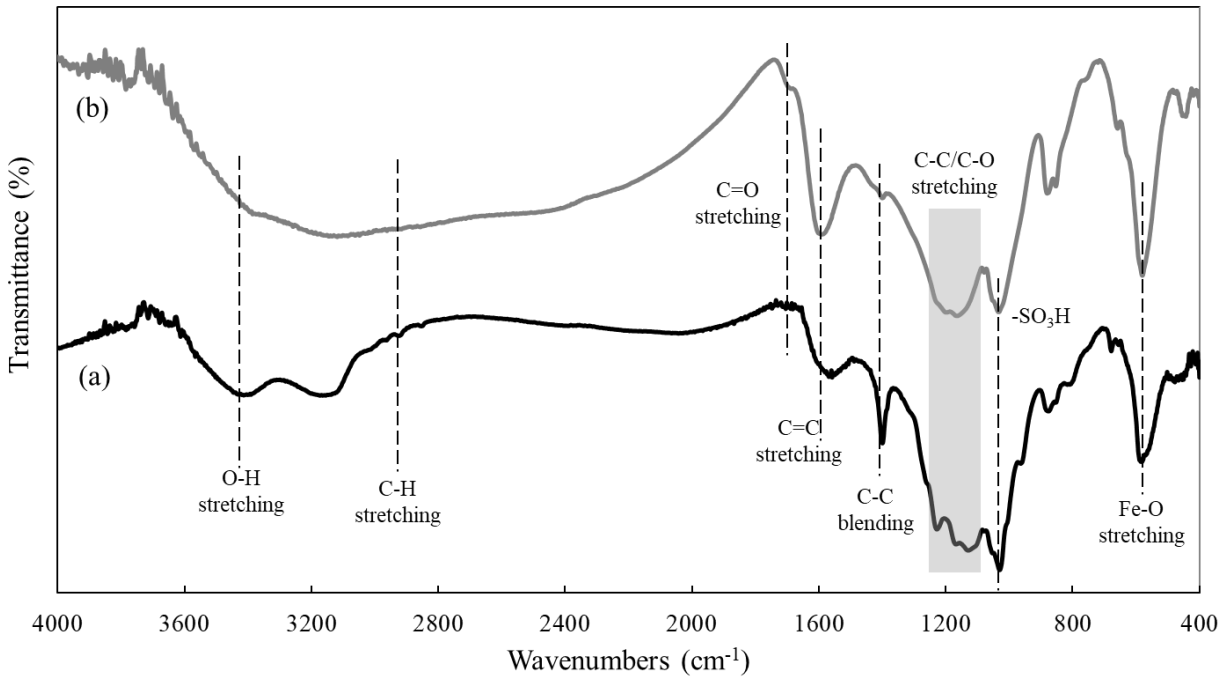

Figure 7. FT-IR spectra of (a) EFB lignin-SO_3H@Fe_3O_4 and (b) commercial lignin-SO_3H@Fe_3O_4.

FT-IR analysis (Figure 7) was conducted to determine the presence of functional groups in sulfonated catalysts, and Figure S3 illustrates the spectra of EFB lignin and commercial lignin. The band of 3413 cm^{-1} was attributed to O-H stretching vibration and indicated the existence of -OH and -COOH groups in both catalysts [34]. During carbonisation, the C=C stretching vibration at 1590

cm^{-1} possibly suggested a higher poly-aromatization for EFB lignin-SO_3H@Fe_3O_4. The absorption at 1032 cm^{-1} was attributed to S=O symmetric stretching and indicated the presence of -SO_3H groups in both catalysts after the sulfonation process [35], while the strong absorption of Fe-O stretching vibration at 581-580 cm^{-1} demonstrated the successful loading of Fe_3O_4 in the two magnetic solid acid catalysts. Suminar et al. studied the lignin-derived carbonaceous catalyst for biodiesel production and showed that the catalyst has SO_3H groups linked to the amorphous structure C-O-S stretching vibration and S=O symmetric stretching [36]. Similarly, the absorption peaks were identified in both lignin-derived magnetic acid catalysts and indicated the same functional groups.

Box-Behnken Optimisation of Esterification Conditions over EFB Lignin-SO_3H@Fe_3O_4 Catalyst

Table 5 and Figure 8 show the experimental and predicted results obtained in the Box-Behnken optimisation of oleic acid esterification at 60 °C over the EFB lignin-SO_3H@Fe_3O_4 catalyst. The model's accuracy was verified by determining the R^2 value, which was found to be 0.9711 (Table 6b). The quadratic model can interpret more than 97.11% of the output response, and the remaining 2.89% is formed from residues. The statistical optimisation gave a quadratic polynomial equation model (Eq. 4) as follows:

$$Y = 81.48 + 4.50x_1 + 4.76x_2 + 2.66x_3 + 2.05x_1x_2 + 2.45x_1x_3 + 0.28x_2x_3 - 1.73x_1^2 - 1.20x_2^2 - 1.20x_3^2 \quad \text{(Eq. 4)}$$

where X_1, X_2 and X_3 referred to the three independent variables, namely catalyst loading, methanol to OA molar ratio and esterification time, respectively (Table 6), while Y was the conversion rate of oleic acid as response.

Table 5. Experimental and predicted results of oleic acid esterification over EFB lignin-SO_3H@Fe_3O_4 catalyst using Box-Behnken methodology.

Std	Run	X_1--Catalyst loading, %	X_2--Methanol: OA	X_3--Duration, min	Y_{test}--Experimental conversion, %	$Y_{predicted}$--Predicted conversion, %
16	1	7	10	120	81.9	81.5
11	2	7	8	150	77.1	76.7
7	3	5	10	150	75.1	74.3
14	4	7	10	120	80.2	81.5
8	5	9	10	150	88.5	88.2
10	6	7	12	90	80.5	80.9
1	7	5	8	120	70.1	71.3
15	8	7	10	120	81.5	81.5
13	9	7	10	120	81.3	81.5
9	10	7	8	90	73.5	71.9
12	11	7	12	150	85.2	86.8
6	12	9	10	90	77.1	77.9
17	13	7	10	120	82.5	81.5
3	14	5	12	120	77.5	76.8
4	15	9	12	120	91.1	89.9
5	16	5	10	90	73.5	73.8
2	17	9	8	120	75.5	76.2

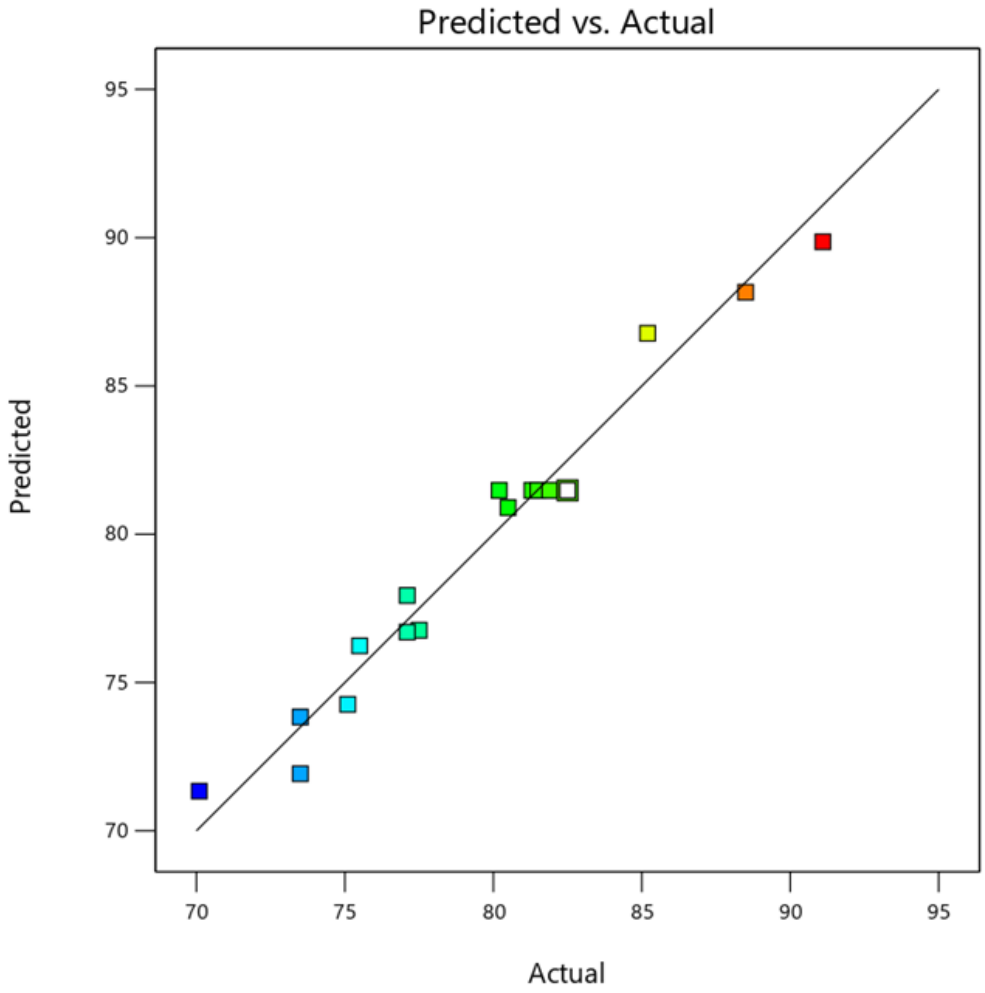

Figure 8. Comparison between actual versus predicted data for esterification rate.

Analysis of variance (ANOVA) was used to evaluate the statistical data, suitability of the quadratic model and investigate the effect of reaction parameters on the response. The ANOVA results for the esterification of oleic acid are shown in Table 6a. The model's accuracy was determined using the regression coefficient, which yielded an R^2 value of 0.941, indicating that more than 94.1% of the output response was significant to the quadratic model (Eq. 4). The remaining 5.9% is attributed to residues. The predicted R^2 of 0.624 is in reasonable agreement with the adjusted R^2 of 0.934. The model is expected to have a good fit, with a regression coefficient value of more than 80%. Table 6b shows the correlation variation (C.V.%) was 1.77%, less than 10%, and the lower C.V.% value indicates a good model fit. The *p*-value obtained from the ANOVA was 0.0001, indicating that all parameters are statistically significant. The results from the ANOVA also clearly indicate that all linear terms, X_1: catalyst loading, X_2: methanol to OA molar ratio, X_3: duration and their quadratic terms: X_1^2, X_2^2 and X_3^2, are significant. A and B were the most significant variables for achieving a higher percentage conversion in the esterification reaction. Regarding interactions, terms with X_1X_2 and X_1X_3 are more significant. The model F-value of 26.14 indicates that the model terms are significant. The Lack of Fit, with a p-value of 0.0746, which is higher than 0.05, implies that the Lack of Fit is insignificant. There is only a 7.46% chance that a Lack of Fit F-value this large could occur due to noise.

Table 6. Significance test (a) and variance analysis (b) of regression coefficients.

(a)

	Sum of squares	df	Mean square	F value	P-value	
Model	468.81	9	52.09	26.14	0.0001	significant
X_1-Catalyst loading	162.00	1	162.00	81.29	< 0.0001	
X_2-MeOH:OA	181.45	1	181.45	91.05	< 0.0001	
X_3-Duration	56.71	1	56.71	28.46	0.0011	
$X_1 X_2$	16.81	1	16.81	8.43	0.0228	
$X_1 X_3$	24.01	1	24.01	12.05	0.0104	
$X_2 X_3$	0.30	1	0.30	0.15	0.7084	
X_1^2	12.57	1	12.57	6.30	0.0403	
X_2^2	6.09	1	6.09	3.06	0.1240	
X_3^2	6.09	1	6.09	3.06	0.1240	
Residual	13.95	7	1.99			
Lack of Fit	11.06	3	3.69	5.11	0.0746	not significant
Pure Error	2.89	4	0.72			
Cor Total	482.76	16				

df = degree of freedom

(b)

Terms	Coefficient	Standard error	t-Stat
Intercept	81.48	0.63	82.97
X_1-Catalyst loading	4.5	0.5	5.68
X_2-Methanol: OA	4.76	0.5	5.94
X_3-Reaction time	2.66	0.5	3.84
$X_1 X_2$	2.05	0.71	3.72
$X_1 X_3$	2.45	0.71	4.12
$X_2 X_3$	0.28	0.71	1.94
X_1^2	-1.73	0.69	-0.1
X_2^2	-1.2	0.69	0.42
X_3^2	-1.2	0.69	0.42
Statistical parameters	Values	Statistical parameters	Values
Standard deviation	1.41	R-Squared	0.97
Mean	80.54	Adjusted R-Squared	0.93
Coefficient of variation (C.V.%)	1.77	Predicted R-Squared	0.62
PRESS	181.51	Adequate Precision	17.11

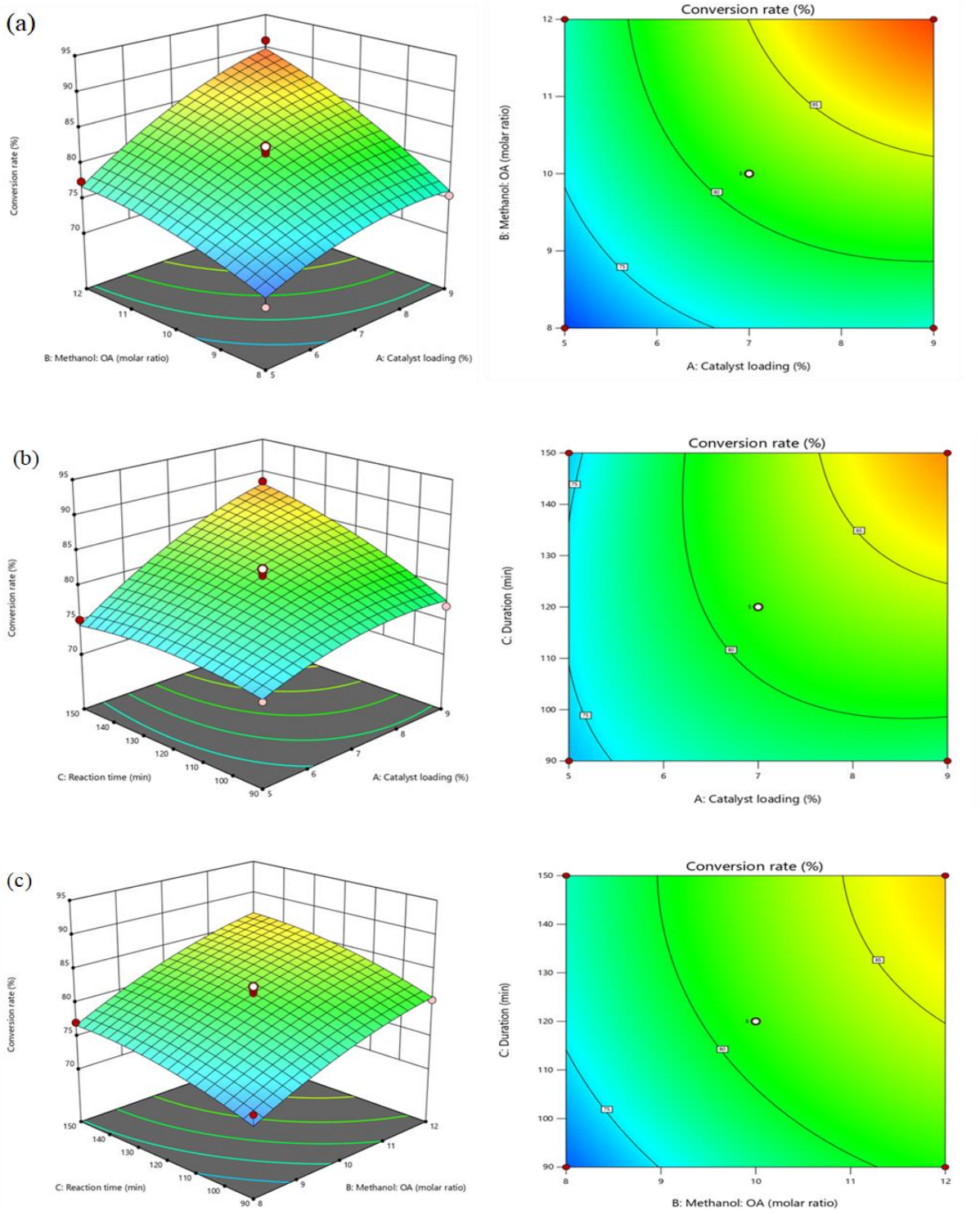

Figure 9. Response surface plots and contour plots of esterification rate over EFB lignin-SO_3H@Fe_3O_4 *vs*. a) catalyst loading and methanol/OA molar ratio, with a fixed duration of 150 min, b) catalyst loading and duration, with a fixed methanol/OA ratio of 10 and c) methanol/OA molar ratio and duration, with catalyst loading of 9 wt%.

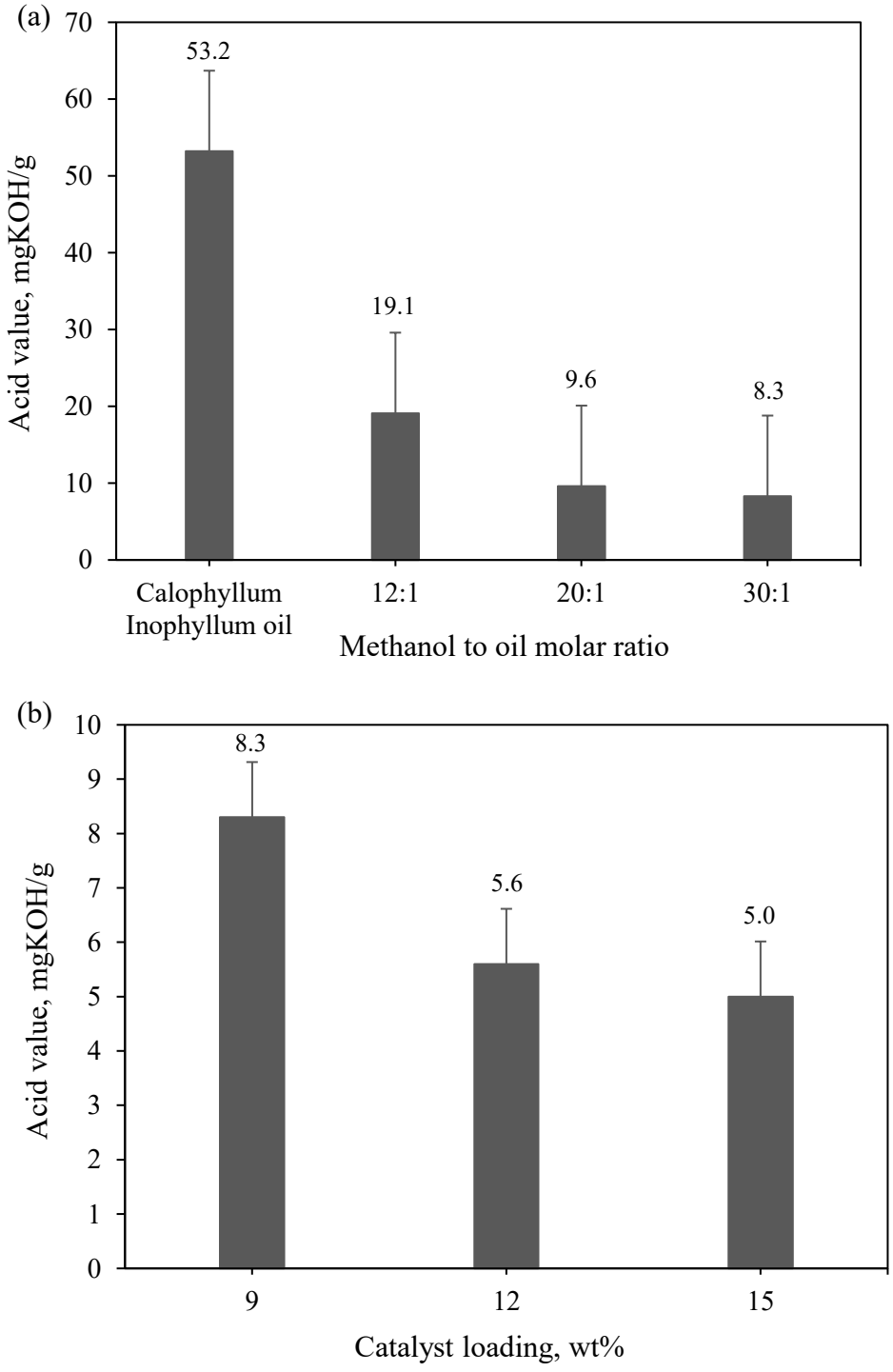

Figure 10. Deacidification of *Calophyllum inophyllum* oil with different (a) methanol to oil molar ratio (Deacidification conditions: 60 °C, 2 h, catalyst loading of 9 wt%) and (b) catalyst loading (Deacidification conditions: 60 °C, 2 h, methanol to oil molar ratio 30).

The interaction of two independent factors on the esterification rate of oleic acid was graphically represented in Figure 9. In Figure 9a, esterification was performed at 60 °C for a fixed duration of 150 min, the increase in methanol to OA molar ratio and catalyst loading contributed to enhance conversion of oleic acid to methyl oleate, which gave the highest yield of 88.5% with methanol to OA molar ratio of 10 and catalyst loading of 9%. The linear term of catalyst loading, with an F-value of 81.29, was identified as the most influential parameter. Hence, the high catalyst loading could enhance the conversion rate; however, the conversion rate was slightly decreased as the F-value was 6.30 for the squared term of catalyst

loading (A^2). It could be reflected in the distribution or interaction at higher concentrations of the heterogeneous catalyst. In Figure 9b, when esterification was performed at 60 °C with a fixed methanol to oil molar ratio of 10, a high amount of catalyst and longer reaction duration benefited the interaction of liquid reactants with solid catalysts, thus increasing the conversion rate. It shows that a high amount of catalyst and longer reaction time exhibited a high conversion rate [37]. The conversion rate decreased as the catalyst loading reduced with a longer reaction time. It could be due to the limited amount of catalyst in the reaction mixture, which allows the reactant to react to the catalyst for a high conversion rate. Moreover, prolonging the reaction time could allow the reactants to interact with the catalyst to increase the conversion rate. Iftitahiyah et al. suggested that the conversion rate improved by extending the reaction time [38]. It further indicates that in the presence of an excess of methanol in the reaction, it is more likely to deactivate the catalyst's active sites, probably by occupying them. Meantime, Manan et al. stated that an increment in the ester conversion rate was observed with the increase in the reaction time [39]. But further prolonging the reaction time by more than 5 h was inadequate for the conversion rate, presumably due to the increase in the water formation as a by-product of the esterification reaction. Thus, the highest conversion was recorded as 88.5% with catalyst loading of 9% for a duration of 150 min.

The esterification rate was plotted against the interaction of methanol to oil molar ratio and duration, as shown in Figure 9c at 60 °C with a fixed catalyst loading of 7%. The esterification rate increased when a lower methanol to OA ratio was executed for a longer reaction duration. Moreover, excess methanol dilutes the oleic acid and catalyst concentration, reducing the interaction between reactants and the catalyst's active sites [40]. Meanwhile, the interaction between excess alcohol and sulfonic groups (-SO_3H) resulted in the formation of sulfonic ester that prevents catalytic efficiency [41]. The limitation in the esterification reaction was caused by the poor accessibility of the catalyst surface with increasing alcohol concentration. As a result, a higher esterification rate was obtained at a methanol to OA ratio of 10 and a reaction duration of 120 min. In summary, it was validated that the optimised reaction parameter conditions were 60 °C, 8.8 wt% catalyst loading, methanol to OA molar ratio of 11.9:1 and reaction time of 148 min with the highest conversion of 92.05%.

Esterification of *Calophyllum inophyllum* Oil using EFB Lignin-SO_3H@Fe_3O_4 Catalyst

CI oil with an acid value of 53.2 mg KOH/g was used to determine the deacidification efficiency of high acid value oil at 60 °C over an EFB lignin-SO_3H@Fe_3O_4 catalyst. The increased methanol usage in the reaction mixture pushed the reaction equilibrium forward to produce more methyl esters [42]. The acid value of CI oil was efficiently reduced to 8.3 mg KOH/g by the esterification treatment within 2 h and using a methanol/oil molar ratio of 30 (Figure 10a). The effect of catalyst loading on the deacidification of CI oil was studied. The acid value was further reduced to 5.0 mg KOH/g by the esterification treatment within 2 h using 15 wt% catalyst loading and methanol/oil molar ratio of 30 (Figure 10b), which is approximately near to the required FFA level of <2±% for subsequent base-catalysed transesterification. The deacidification rate was calculated as 90.6%. Figure S4 shows the GC spectrum of esterified CI oil, indicating the successful forming of methyl esters.

CONCLUSION

This study developed a three-step methodology, including hydrothermal carbonisation of EFB lignin and commercial lignin with Fe(OH)x, calcination and sulfuric acid sulfonation to synthesise lignin-derived magnetic solid acid catalysts. The catalyst showed relatively higher surface acidity (1.50 -2.20 mmol SO_3H/g) and performed well in the catalytic esterification of oleic acid with methanol. A high esterification rate of >83% was still achieved after 5 cycles of esterification at 60 °C within 2 h when using commercial lignin-SO_3H@Fe_3O_4 as the catalyst. This meant that the catalyst activity from the 2nd to 5th cycle only decreased by 6.3%, a better result than that previously reported in other literature. The preparation of commercial lignin-SO_3H@Fe_3O_4 was optimised by the orthogonal method, which exhibited the best activity under the conditions: lignin loading of 6 g, hydrothermal carbonisation duration of 12 h and calcination at 500 °C for 90 min. Esterification parameters were also optimised over EFB lignin-SO_3H@Fe_3O_4 using Box-Behnken methodology, which gave the optimised conditions: 60 °C, 8.8 wt% catalyst loading, methanol to oleic acid molar ratio of 11.9:1 and reaction time of 148 min with the highest conversion of 92.05%. EFB lignin-SO_3H@Fe_3O_4 was further tested in the esterification of *Calophyllum Inophyllum* oil containing very high free fatty acid content. The catalyst exhibited a deacidification efficiency of 84.3% with an enhanced methanol-to-oil molar ratio of 30:1. In summary, the prepared solid catalyst possessed good properties such as strong magnetism, high surface acidity, and improved reusability, which made the catalyst a potential candidate to be used as a green, effective and practical heterogeneous catalyst in biodiesel production.

ACKNOWLEDGEMENTS

The authors want to acknowledge the financial support and facilities provided by the Chinese Academy of Sciences, Xishuangbanna Tropical Botanical Garden, Kunming, China. We also thank the Yunnan Revitalization Talent Support Program (No. XDYC-QNRC-2022-0071) and the Ministry of Education

(MOE)'s Fundamental Research Grant Scheme (FRGS/1/2018/STG07/UNITEN/02/3) for financial support.

REFERENCES

1. Krishnan, S. G., Pua, F. L. and Zhang, F. (2021) A review of magnetic solid catalyst development for sustainable biodiesel production. *Biomass and Bioenergy*, **149**, 106099.

2. Lopresto, C. G. (2025) Sustainable biodiesel production from waste cooking oils for energetically independent small communities: an overview. *International Journal of Environmental Science and Technology*, **22(3)**, 1953–1974.

3. Monika, Banga, S. and Pathak, V. V. (2023) Biodiesel production from waste cooking oil: A comprehensive review on the application of heterogenous catalysts. *Energy Nexus*, **10**.

4. Farouk, S. M., Tayeb, A. M., Abdel-Hamid, S. M. S. and Osman, R. M. (2024) Recent advances in transesterification for sustainable biodiesel production, challenges, and prospects: a comprehensive review. *Environmental Science and Pollution Research*, **31(9)**, 12722–12747.

5. Jain, M., Chandrakant, U., Orsat, V. and Raghavan, V. (2018) A review on assessment of biodiesel production methodologies from Calophyllum inophyllum seed oil. *Industrial Crops and Products*, **114**, 28–44.

6. Zhang, F., Tian, X., Shah, M. and Yang, W. (2017) Synthesis of magnetic carbonaceous acids derived from hydrolysates of Jatropha hulls for catalytic biodiesel production. *RSC Advances*, **7(19)**, 11403–11413.

7. Pandey, V., Badruddin, I. A., Zuber, M. and Kamangar, S. (2025) Combustion analysis of CI engine fuelled with calophyllum inophyllum methyl ester biodiesel and CeO2 nanoparticle additives. *Scientific Reports*, **15(1)**.

8. Wang, A., Sudarsanam, P., Xu, Y., Zhang, H., Li, H. and Yang, S. (2020) Functionalized magnetic nanosized materials for efficient biodiesel synthesis via acid-base/enzyme catalysis. *Green Chemistry*, **22(10)**, 2977–3012.

9. Konwar, L. J., Mäki-Arvela, P. and Mikkola, J. P. (2019) SO3H-Containing Functional Carbon Materials: Synthesis, Structure, and Acid Catalysis. *Chemical Reviews*, **119(22)**, 11576–11630.

10. Gerami, M., Farahi, M. and Karami, B. (2025) Magnetic lignin-supported sulfonic acid ionic liquid: a novel catalyst for synthesis of 2-amino-4-aryl-4 H -benzo[f]chromen-3-carbonitrile derivatives. *RSC Advances*, **15(54)**, 46380–46390.

11. Pua, F. L., Fang, Z., Zakaria, S., Guo, F. and Chia, C. (2012) Direct production of biodiesel from high-acid value Jatropha oil with solid acid catalyst derived from lignin. *Biotechnology for Biofuels*, **5(1)**, 66.

12. Dechakhumwat, S., Hongmanorom, P., Thunyaratchatanon, C., Smith, S. M., Boonyuen, S. and Luengnaruemitchai, A. (2020) Catalytic activity of heterogeneous acid catalysts derived from corncob in the esterification of oleic acid with methanol. *Renewable Energy*, **148**, 897–906.

13. Jabarullah, N. H., Othman, R., Kamal, A. S., Salleh, M. R. M., Urbański, M. and Liszewski, W. (2022) The synthesis of biographene oxide from the graphitic structure of PKS, EFB and OPF. *Acta Montanistica Slovaca*, **27(4)**, 864–875.

14. Jahi, N., Othaman, R., Lazim, A. M. and Ramli, S. (2020) Empty fruit bunch cellulose based sorbent for oil sorption in palm oil mill effluent. *Sains Malaysiana*, **49(9)**, 2323–2333.

15. Hafyan, R. H., Bhullar, L. K., Mahadzir, S., Bilad, M. R., Hadi Nordin, N. A., Hakim Wirzal, M. D., Putra, Z. A. and Abdullah, B. (2020) Integrated biorefinery of empty fruit bunch from palm oil industries to produce valuable biochemicals. *Processes*, **8(7)**.

16. Hu, S., Huang, J., Huang, D., Li, P., Tang, J. and Meng, F. (2021) Increased flexibility to improve the catalytic performance of carbon-based solid acid catalysts. *Green Processing and Synthesis*, **10(1)**, 687–699.

17. Zhang, B., Gao, M., Geng, J., Cheng, Y., Wang, X., Wu, C., Wang, Q. and Cheung, S. M. (2021) Catalytic performance and deactivation mechanism of a one-step sulfonated carbon-based solid-acid catalyst in an esterification reaction. *Renewable Energy*, **164**, 824–832.

18. Zhang, Y., Li, W., Wang, J., Jin, J., Zhang, Y., Cheng, J. and Zhang, Q. (2023) Advancement in utilization of magnetic catalysts for production of sustainable biofuels. *Frontiers in Chemistry*, **10**.

19. Hassan, A. H., Zainol, M. M., Zainuddin, K. R., Saperi, N. Q., Mohammed Yussuf, M. A., Rahman, N. A. and Mohd Nor Azman, N. A. N. (2022) Sulfonated Carbon Catalyst Prepared from Calcination of Lignin for Ethyl Levulinate Synthesis via Ethanolysis of Levulinic Acid. *Chemical Engineering Transactions*, **97**, 307–312.

20. Wang, Y. T., Yang, X. X., Xu, J., Wang, H. L., Wang, Z. B., Zhang, L., Wang, S. L. and Liang, J. L. (2019) Biodiesel production from esterification of oleic acid by a sulfonated magnetic solid acid catalyst. *Renewable Energy*, **139**, 688–695.

21. Krishnan, S. G., Pua, F. L. and Fan, Z. (2023) Effect of Chemical Pre-Treatment on the Catalytic Performance of Oil Palm EFB Fibre Supported Magnetic Acid Catalyst. *Sustainability*, **15(11)**.

22. Laksono, S. E., Suryandari, A. S., Widiyastuti, W., Nurtono, T. and Setyawan, H. (2024) Effect of Sulfonating Agent on Esterification Reaction Using Aerogel Carbon Based Support Material. *Engineering Chemistry*, **7**, 41–50.

23. Basumatary, S. F., Das, B., Das, B. K., Hoque, M., Brahma, S., Basumatary, B., Patir, K. and Basumatary, S. (2024) Recent advances in magnetic solid catalysts: Synthesis, stabilization and application in cleaner production of biodiesel. *Energy Nexus*, **15**.

24. Yu, H., Niu, S., Bai, T., Tang, X. and Lu, C. (2018) Microwave-assisted preparation of coal-based heterogeneous acid catalyst and its catalytic performance in esterification. *Journal of Cleaner Production*, **183**, 67–76.

25. Niu, S., Ning, Y., Lu, C., Han, K., Yu, H. and Zhou, Y. (2018) Esterification of oleic acid to produce biodiesel catalyzed by sulfonated activated carbon from bamboo. *Energy Conversion and Management*, **163**, 59–65.

26. Jenie, S. N. A., Kristiani, A., Sudiyarmanto, Khaerudini, D. S. and Takeishi, K. (2020) Sulfonated magnetic nanobiochar as heterogeneous acid catalyst for esterification reaction. *Journal of Environmental Chemical Engineering*, **8(4)**, 103912.

27. Yang, Y. T., Yang, X. X., Wang, Y. T., Luo, J., Zhang, F., Yang, W. J. and Chen, J. H. (2018) Alcohothermal carbonization of biomass to prepare novel solid catalysts for oleic acid esterification. *Fuel*, **219**, 166–175.

28. Tingting, L., Yang, W., Baile, W., Fan, Y., Nadezda, V. T. and Markus, A. (2023) 'Green-to-Green': Iron oxides embedded in lignin-based carbon scaffolds for water remediation via oxidation excluding free-radical pathways. *Journal of Hazardous Materials*, **442**, 130070.

29. Sangsiri, P., Laosiripojana, N., Laosiripojana, W. and Daorattanachai, P. (2022) Activity of a Sulfonated Carbon-Based Catalyst Derived from Organosolv Lignin toward Esterification of Stearic Acid under Near-Critical Alcohol Conditions. *ACS Omega*, **7(44)**, 40025–40033.

30. Zhang, F., Fang, Z. and Wang, Y. T. (2015) Biodiesel production direct from high acid value oil with a novel magnetic carbonaceous acid. *Applied Energy*, **155**, 637–647.

31. Wang, A., Li, H., Pan, H., Zhang, H., Xu, F., Yu, Z. and Yang, S. (2018) Efficient and green production of biodiesel catalyzed by recyclable biomass-derived magnetic acids. *Fuel Processing Technology*, **181**, 259–267.

32. Adhikari, S., Hood, Z., Gallego, N. and Contescu, C. (2018) Lignin-Derived Carbon Fibers as Efficient Heterogeneous Solid Acid Catalysts for Esterification of Oleic Acid. *MRS Advances*, **3**, 2865–2873.

33. Ma, Y. Z., Zheng, D. F., Mo, Z. Y., Dong, R. J. and Qiu, X. Q. (2018) Magnetic lignin-based carbon nanoparticles and the adsorption for removal of methyl orange. *Colloids and Surfaces A: Physicochemical and Engineering Aspects*, **559**, 226–234.

34. Sripada, S. and Kastner, J. R. (2023) Continuous Catalytic Esterification Using a Solid Acid Activated Carbon Monolith: Comparison of Granular and Monolith forms with a Commercial Catalyst. *Chemical Engineering Journal*, **476**, 146586.

35. Hamilton, A., Pains Duarte, M. and Naccache, R. (2025) Corn Stover Lignin as a Solid Acid Catalyst for the Esterification of Oleic Acid. *Particle and Particle Systems Characterization*, **42(3)**.

36. Suminar, D. R., Pribadi, C. Z., Fitriana, Q. R., Andrijanto, E., Permana, M. D., Eddy, D. R. and Rahayu, I. (2024) Corncob waste derived carbon with sulfonic acid group: An efficient heterogeneous catalyst for production of ethyl levulinate as biodiesel additives. *Heliyon*, **10(18)**.

37. Quah, R. V., Tan, Y. H., Mubarak, N. M., Kansedo, J., Khalid, M., Abdullah, E. C. and Abdullah, M. O. (2020) Magnetic biochar derived from waste palm kernel shell for biodiesel production via sulfonation. *Waste Management*, **118**, 626–636.

38. Iftitahiyah, V. N., Prasetyoko, D., Hartati, Ni'Mah, Y. L., Bahruji, H. and Nur, H. (2019) Esterification of acetic acid and benzyl alcohol over Zeolite HX produced from bangka belitung kaolin. *Malaysian Journal of Analytical Sciences*, **23(3)**, 524–533.

39. Manan, F. M. A., Attan, N., Zakaria, Z., Keyon, A. S. A. and Wahab, R. A. (2018) Enzymatic esterification of eugenol and benzoic acid by a novel chitosan-chitin nanowhiskers supported Rhizomucor miehei lipase: Process optimization and kinetic assessments. *Enzyme and Microbial Technology*, **108**, 42–52.

40. Zhang, B., Gao, M., Geng, J., Cheng, Y., Wang, X., Wu, C., Wang, Q. and Cheung, S. M. (2021) Catalytic performance and deactivation mechanism of a one-step sulfonated carbon-based solid-acid catalyst in an esterification reaction. *Renewable Energy*, **164**, 824–832.

41. Anekwe, I. M. S. and Isa, Y. M. (2025) Unlocking catalytic longevity: a critical review of catalyst deactivation pathways and regeneration technologies. *Energy Advances*, **4(9)**, 1075–1113.

42. Agapay, R. C., Liu, H. C., Ju, Y. H., Go, A. W., Angkawijaya, A. E., Nguyen, P. L. T., Truong, C. T. and Quijote, K. L. (2021) Synthesis and Initial Evaluation of Solid Acid Catalyst Derived from Spent Coffee Grounds for the Esterification of Oleic Acid and Methanol. *Waste and Biomass Valorization*, **12**, 4387–4397.